STATISTICAL SHAPE ANALYSIS FOR COMPUTER AIDED FACIAL DEFORMITY DETECTION

Mohd Bakery Md Hussin, Halim Setan, Zulkepli Majid and Deni Suwardhi

Medical Imaging Research Group, Faculty of Geoinformation Science and Engineering
Universiti Teknologi Malaysia, 81310 UTM Skudai, Johor, Malaysia
Tel: +607-5530380
E-Mail: bakery@fksg.utm.my

Abstract

This paper describes craniofacial medical application, with the emphasis on the comparison of normal and abnormal facial data by using statistical shape analysis method to classify the data sets. The data consists of 3D laser scans of mannequin faces. The normal facial dataset is based on the mannequin. The distance between two landmarks and angle between three landmarks are used as the reference to determine whether the facial datasets are normal or abnormal with respect to the normal facial dataset. The statistical shape analysis is a useful tool for facial analysis after the treatment of facial deformity.

Keywords: *Standard Deviation, Probability*

1.0 INTRODUCTION

In this study, the facial deformity determination uses the distance and angle measurements based on mannequin landmarks data. From these two measurements, the scale of the normality of facial data is obtained from the probability value of the two measurements. There are 27 landmarks on each mannequin (and total of 30 mannequins were used). VIVID910 laser scanner and RapidForm software were employed to scan the mannequin and to get the coordinates of the mannequin.

The standard deviation is the “mean of the mean”, and also called normal distribution. A normal distribution of data means that most of the examples in a set of data are close to the “average”. The probability is the possible outcomes of the given events together with the outcomes' relative likelihoods and distributions. Probability is used to mean the chance that a particular event (or set of events) will occur expressed on a linear scale from 0 (impossibility) to 1 (certainty), also expressed as a percentage between 0 and 100%. If the probability value is between 0 and 1, the datasets is considered normal.

2.0 METHOD

The data consists of 3D scans taken from the same 30 mannequins. The distance and angle measurements of the mannequin (Figure 1) were based on the landmarks shown in Table 1 and Table 2.

Table 1: Distance and angle measurement landmarks

Distance Measurement	Angle Measurement
tr-pg	sci(r) - tr - sci(l)
tr-g	ex(r) - sci(r) - en(r)
ls-sl	en(l) - sci(l) - ex(l)
ch(r)-ch(l)	en(r) - s - en(l)
ex-en	ch(r) - ls - ch(l)

ex(r)-ex(l)	ch(r) - pg - ch(l)
en(r)-en(l)	sba(r) - ex(r) - ch(r)
sa-sba	sba(l) - ex(l) - ch(l)
go(r)-go(l)	sba(r) - sa(r) - ex(r)
tr-prn	sba(l) - sa(l) - ex(l)

Table 2: Landmark, name and landmark definition

No	Landmark	Name	Definition
1	tr	Trichion	Mid point of the hairline.
2	g	Glabella	The most prominent midline point between the eyebrows and is identical to the bony glabella on the frontal bone.
3	s	Sellion	The deepest landmark located on the bottom of the nasofrontal angle.
4	prn	Pronasale	The most protruded point of the nasal tip
5	ls	Labiale superius	The midpoint of the vermilion border of the upper lip.
6	sl	Sublabiale	The lower border of the lower lip or the upper border of the chin.
7	pg	Pogion	The most anterior midpoint of the chin
8	sci-r	Superciliare (right)	The highest point on the upper margin of the middle portion of the eyebrow (right).
9	sci-l	Superciliare (left)	The highest point on the upper margin of the middle portion of the eyebrow (left).
10	en-r	Endocanthion (right)	The inner corner of the eye fissure where the eyelids meet, not the caruncles (the red eminences at the medial angles of the eyes) (right).
11	en-l	Endocanthion (left)	The inner corner of the eye fissure where the eyelids meet, not the caruncles (the red eminences at the medial angles of the eyes) (left).
12	ex-r	Exocanthion (right)	The outer corner of the eye fissure where the eyelids meet (right).
13	ex-l	Exocanthion (left)	The outer corner of the eye fissure where the eyelids meet (left).
14	ch-r	Cheilion (right)	The outer corner of the mouth where the outer edges of the upper and lower vermilions meet (right)
15	ch-l	Cheilion (left)	The outer corner of the mouth where the outer edges of the upper and lower vermilions meet (left)
16	sa-r	Superaurable (right)	The highest point of the free margin of the ear (right).
17	sa-l	Superaurable (left)	The highest point of the free margin of the ear (right).
18	t-r	Tragion (right)	The notch on the upper margin or the tragus (right).
19	t-l	Tragion (left)	The notch on the upper margin or the tragus (left).

20	sba-r	Subaurale (right)	The lowest point on the free margin of the ear lobe (right).
21	sba-l	Subaurale (left)	The lowest point on the free margin of the ear lobe (left).
22	go-r	Gonion (right)	The most lateral point at the angle of the mandible (right).
23	go-l	Gonion (left)	The most lateral point at the angle of the mandible (left).
24	ft-r	Frontotemporale (right)	The point on each side of the forehead, laterally from the elevation of the linea temporalis (right).
25	ft-l	Frontotemporale (left)	The point on each side of the forehead, laterally from the elevation of the linea temporalis (left).
26	zy-r	Zygion (right)	The most lateral point on the zygomatique (right).
27	zy-l	Zygion (left)	The most lateral point on the zygomatique (left).

Before the scanning process, all 30 mannequins were marked with 3mm targets (i.e. to identify 27 landmarks for each mannequin). The laser scanner provides 3D coordinates of each mannequin, and Rapidform software gives 3D coordinates of the landmarks.

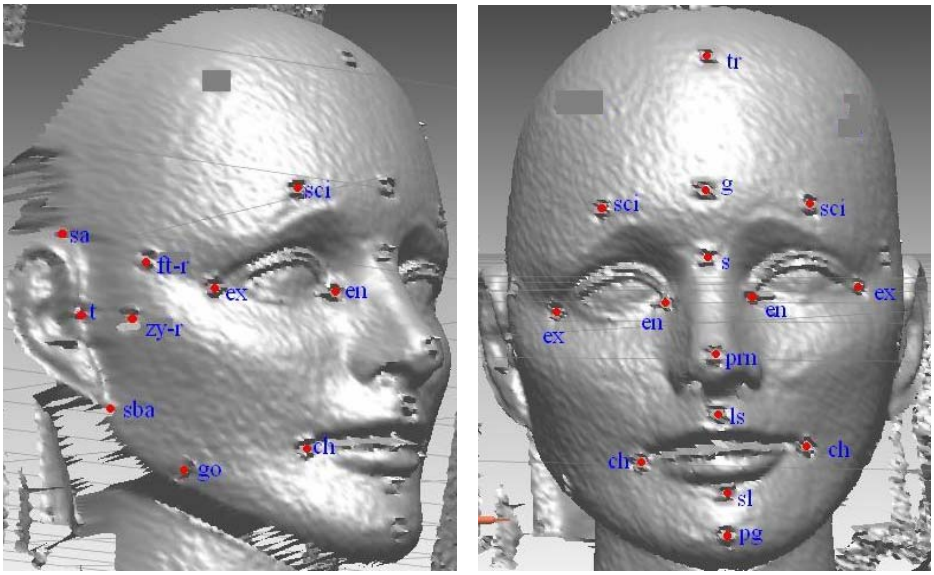

Figure 1: Mannequin image scanned by laser scanner and RapidForm software with landmarks

The distance and angle were measured using the tool in RapidForm software. There were ten distances and ten angles measurement (Table 1) for every mannequin. The mean and standard deviation for all measurements, and the probability value were computed. The probability value can be used to determine whether any dataset is normal or abnormal. According to Table 4 and Table 6, the abnormality also can be defined by the lower and upper measurements values.

3.0 RESULT AND CONCLUSIONS

Table 3: One-Sample Statistics Angle Measurements

One-Sample Statistics Angle Measurements				
	N	**Mean**	**Std. Deviation**	**Std. Error Mean**
sci(r) - tr - sci(l)	30	67.29077067	2.175115881	0.397120011
ex(r) - sci(r) - en(r)	30	63.24779433	2.91540341	0.532277404
en(l) - sci(l) - ex(l)	30	69.766935	3.856908886	0.704172
en(r) - s - en(l)	30	86.37607033	4.004428898	0.731105346
ch(r) - ls - ch(l)	30	94.321299	2.065189157	0.377050229
ch(r) - pg - ch(l)	30	80.883488	1.88573926	0.34428731
sba(r) - ex(r) - ch(r)	30	72.22714833	1.909611478	0.348645761
sba(l) - ex(l) - ch(l)	30	69.83639467	2.432414437	0.444096086
sba(r) - sa(r) - ex(r)	30	51.79632067	1.97565826	0.360704198
sba(l) - sa(l) - ex(l)	30	65.306863	2.625482071	0.479345251

Table 3 above shows the mean and standard deviation of angle measurements. Based on the mean and standard deviation values, the probabilistic values or confidence intervals of the difference angle measurement were computed (Table 4). The upper and lower limits show the maximum and minimum values of the normal landmarks angle measurement.

Table 4: 95% Confidence Interval of the Difference Angle Measurement

95% Confidence Interval of the Difference		
	Lower	**Upper**
sci(r) - tr - sci(l)	66.47856905	68.10297228
ex(r) - sci(r) - en(r)	62.15916481	64.33642386
en(l) - sci(l) - ex(l)	68.32674155	71.20712845
en(r) - s - en(l)	84.88079201	87.87134866
ch(r) - ls - ch(l)	93.5501447	95.0924533
ch(r) - pg - ch(l)	80.17934139	81.58763461
sba(r) - ex(r) - ch(r)	71.51408769	72.94020898
sba(l) - ex(l) - ch(l)	68.92811619	70.74467314
sba(r) - sa(r) - ex(r)	51.05859775	52.53404359
sba(l) - sa(l) - ex(l)	64.32649188	66.28723412

Table 5: One-Sample Statistics Distance Measurements

One-Sample Statistics Distance Measurements				
	N	**Mean**	**Std. Deviation**	**Std. Error Mean**
tr-pg	30	158.960133	2.2256923	0.4063540
tr-g	30	51.262067	1.4055313	.2566137
ls-sl	30	26.329767	1.2062598	.2202319
ch(r)-ch(l)	30	54.670767	1.8100133	.3304617
ex-en	30	38.751067	2.0981564	.3830692
ex(r)-ex(l)	30	98.629000	1.3168822	.2404287
en(r)-en(l)	30	28.902667	1.1331584	.2068855
sa-sba	30	61.694850	1.7605496	.3214309
go(r)-go(l)	30	100.491000	2.4591498	.4489773
tr-prn	30	108.178133	1.5855675	.2894837

Table 5 and Table 6 show the mean and standard deviation of distance measurements, and the confidence interval of the difference distance measurement. The upper and lower limits show the maximum and minimum value of the normal landmarks distance measurement.

Table 6: 95% Confidence Interval of the Difference Distance Measurements

95% Confidence Interval of the Difference		
	Lower	**Upper**
tr-pg	158.129	159.7912
tr-g	50.73723	51.7869
ls-sl	25.87934	26.78019
ch(r)-ch(l)	53.9949	55.34664
ex-en	37.9676	39.53453
ex(r)-ex(l)	98.13727	99.12073
en(r)-en(l)	28.47954	29.32579
sa-sba	61.03745	62.35225
go(r)-go(l)	99.57274	101.4093
tr-prn	107.5861	108.7702

ACKNOWLEDGEMENTS

This research is part of a Prioritized Research (PR) IRPA Vote 75437 sponsored by Ministry of Science, Technology and Innovation Malaysia (MOSTI). The PR involves Universiti Teknologi Malaysia (UTM), Standard & Industrial Research Industrial Malaysia (SIRIM), and Universiti Sains Malaysia (USM).

REFERENCE

1. Fred L. Bookstein (1991). Morphometric Tools for Landmark Data. New York: Camridge University Press.

2. Leslie G. Farkas (1994). Anthropometry of the Head and Face. New York: Raven Press Ltd.

3. Gerhard H. Bendels, Reinhard Klein, Mandana Samimi, Alfred Schmitz (2005). Statistical Shape Analysis for Computer Aided Spine Deformity Detection.

4. Eric Bardinet, Laurent D. Cohen, Nicholas Ayache (1996). A Parametric Deformable Model to Fit Unstructured 3D Data.

5. Erwin Keeve, Sabine Girod, Ron Kikinis, Bernard Girod (1998). Deformable Modeling of Facial Tissue for Craniofacial Surgery Simulation.

6. Jean-Philippe Thirion, Guillaume Calmon (1999). Deformation Analysis ti Detect and Quantify Active Lesions in Three-Dimensional Medical Image Sequences.

7. http://mathworld.wolfram.com